International Journal of Material and Mechanical Engineering, 2012, 1: 38-43
Published Online May 2012

www.ijm-me.org

Study on Synthesis and Optical Properties of ZnO Hierarchical Nanostructures by Hydrothermal Method

Jing Zhang, Daqiang Gao, Guijin Yang, Zhonghua Zhu, Jinlin Zhang, Zhenhua Shi
Key Laboratory for Magnetism and Magnetic Materials of MOE, Lanzhou University, Lanzhou 730000, P. R. China
E-mail: gaodq@lzu.edu.cn

(Abstract) Different ZnO nanostructures are prepared by a two-step hydrothermal method. X-ray diffraction results show that all samples are the typical hexagonal wurtzite structure without any other new phase. SEM and TEM images show that the morphology of the films can be controlled from hexagonal nanorods (irregular/regular) to hierarchical nanostructure (nanorods covered by nanoflakes) through regulating the concentration of the solutes. The intensity of A1(LO) in Raman spectra caused by defects monotonously enhances with the increase of the moles. Additionally, the UV-vis absorption spectra were also measured.

Keywords: Hierarchical Zno Nanostructures; Nanostructures and Morphology; the Optical Properties

1. INTRODUCTION

Over the past several years, the synthesis of nanomaterials with well-defined architectures has attracted great attention because of the potential uses of the nanostructures as building blocks for various nanodevices and nanosystems [1, 2, 3]. Spontaneous formation of nanostructures provides not only a deeper understanding of material growth, but also functional materials for advanced technological applications [1, 4].

Various metal-oxide nanostructures, such as nanowires, nanorods, nanotubes, and nano-colloids have been receiving increased attention because of their wide applications in waveguides, solar cells, blue-UV light-emitting diodes (LEDs), transparent transistors, and sensors [5]. Among all kinds of metal-oxide materials, zinc oxide (ZnO) is an important material for devices that require good performance at room temperature (RT), because ZnO is an n-type wide direct band gap oxide semiconductor material with a band gap energy of 3.37 eV, a high excision binding energy of 60 meV at RT, and also good stability in ambient environments [6, 7, 8, 9], which is a versatile material with potential applications in optical and optoelectronic devices: paints, ceramics, catalysts, varsities, gas sensing, light-emitting devices, and solar cells [10, 11, 12].

Previous reports have described a diverse range of ZnO nanostructures synthesized by various techniques, including nanorods prepared by a one-step aqueous chemical method [13], nanoflowers by a hydrothermal method [14], nanowires arrays synthesized by a post-growth hydrothermal treatment and thermal annealing [7], nanotubulars, nanotrees, and micro sphericals via a polymer-templated hydrothermal growth method [5], microstars with six arms prepared by a solution method [6], microdumbbells by using a diamond-anvil-cell technique [15], multi-layer nanosheets obtained by annealing [4], nanoribbons via a thermal evaporation [4] and so on. It had been shown that the properties of the prepared ZnO samples strongly depend on its nanostructures and morphologies such as size, shape, and orientation from above reports. Most of these recent investigations, however, have been limited to the synthesis and application of ZnO structures with a simplex geometry, studies on hierarchical ZnO structures with novel properties remain still difficult and have been rarely reported.

Although all kinds of ways were used for preparing different nanostructures and morphologies of ZnO, we chose an environmentally friendly hydrothermal method due to the possibility of impurity incorporation [16]. Besides, ZnO prepared by this method has the well crystalline phase, which benefits to thermal stability of the nanosized materials [7, 5, 16, 17].

In this study, we report the two-step hydrothermal method for synthesizing hierarchical ZnO nanostructures on glass substrates. It should be noted that the concentration of the solutes plays a crucial role in the formation of ZnO nanostructures, that is, ZnO shows distinct morphologies in the different moles (M) of solutes: from simple nanorods to nanorods covered by nanoflakes. So we found a simple way to control the nanostructures and morphologies of ZnO films.

2. EXPERIMENTAL SECTION

2.1. Synthesis of ZnO Films

All the chemical reagents used in our experiments are the

analytical grade. Hierarchical ZnO nanostructures were prepared by the two-step hydrothermal synthesis.

At first, the ZnO buffer layers were deposited on glass substrates by a sol-gel method [18]: Prior to deposition, the glass substrates were rinsed in distilled water and cleaned ultrasonically in ethanol and then acetone for removing organic impurities, zinc acetate dihydrate [Zn(CH3COO)2·2H2O] was dissolved in a mixture of 2-methoxyethanol (C3H8O2) and monoethanolamine (MEA, C2H7NO) which served as the solvent and stabilizer, respectively, while the concentration of zinc acetate was 0.75 M and the molar ratio of MEA to zinc acetate was maintained at 1.0. The resultant solution was stirred at 60 ℃ for 4 h and then aged for 48 h. The ready solution was then deposited on glass substrates cleaned using the spin-coating technique at 3000 rpm for 30 s. The as-deposited films were immediately placed into a furnace of 300 ℃ and holded for 10 min. The deposition and preheating processes were repeated for 4 times in order to get an appropriate ZnO buffer layer. Thereafter, the ZnO buffer layers were heated in the air to 500 ℃ from RT, hold at 500 ℃ for 1 h, and cooled in furnace to RT.

After prepared the ZnO buffer layers, a typical hydrothermal synthesis of grown ZnO film was carried out by immersing the ZnO-buffer-layer/glass substrate using a teflon-lined stainless steel autoclave of 50 mL capacity full of the same M of zinc nitrate [Zn(NO3)2] (0.005 M) and hexamethylenetetramine (HMT, C6H12N4, 0.005 M) solutions, and the autoclave was contained at 90 ℃ for 6 h. After the autoclave was allowed to air cool to RT, the film was removed, rinsed with deionizer water and dried in the air.

In order to evaluate the effects of concentration of the solvent on the nanostructures and morphologies of grown ZnO nanostructures, the ZnO buffer layers were immersed in the different-mole solutions of the Zn(NO3)2 and HMT mole of 0.005, 0.01, 0.15, and 0.2 M, so the four different grown ZnO nanostructures were obtained. A schematic diagram of the hydrothermal grown ZnO film on ZnO-buffer-layer/glass substrates is shown in Figure 1.

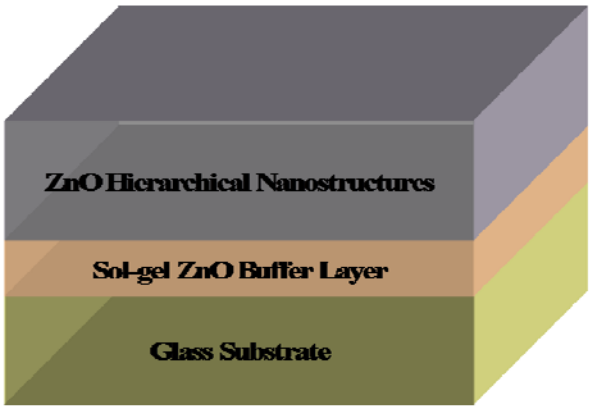

Figure 1. (Color online) The schematic diagram of hierarchical ZnO nanostructures on the ZnO-butter-layer/glass substrate.

2.2. Characterization

The morphologies of samples were characterized by scanning electron microscope (SEM, Hitachi S-4800), transmission electron microscope and high-resolution transmission electron microscope (TEM,TecnaiTM G2 F30, FEI, USA).Selected area electron diffraction (SAED) and X-ray diffraction (XRD, X' Pert PRO PHILIPS with Cu Kα radiation) were employed to study the structure of the samples. The vibration properties were characterized by the Raman scattering spectra measurement, which was performed on a Jobin-Yvon LabRam HR80 spectrometer with a 325 nm line of Torus 50 mW diode-pumped solid-state laser under backscattering geometry. Light absorption property was measured using a UV-vis spectrophotometer (JASCO, UV-550).

3. RESULTS AND DISCUSSION

3.1. SEM

Figure 2 shows some typical SEM images of the grown ZnO nanostructures (*M*=0.005, 0.01, 0.1, 0.2 M). The ZnO buffer layer on glass substrate is made of Nan particles[18] (not shown here), which is very different from the surface morphologies of the grown ZnO nanostructures (nanorods or nanoflates), so it's sure that the grown ZnO nanostructures are successfully prepared on the ZnO-buffer-layer/glass substrates.

From **Figure 2a** and **Figure 2b**, we can see that the ZnO nanostructures (*M*=0.005 M) are made of irregular nanorods which are worse-aligned, rough shape, and disorder. **Figure 2c** and **Figure 2d** show that the ZnO nanostructures (*M*=0.01M) present well-aligned regular hexagonal nanorods, the diameter of the nanorods is ranging between 60 and 150 nm, and the average diameter is about 100 nm. The hexagonal nanorods provide the explicit proof that the nanorods grow along the c-axis direction on the ZnO-buffer-layer/glass substrate, shown in the inset of **Figure 2d**. **Figure 2e** and **Figure 2f** display that the morphology of ZnO (*M*=0.1 M) is the hierarchical nanostructure: internally, the nanorods are straight with the smooth top and hexagon-shaped columnar structure, growing along the c-axis direction as the same as **Figure 2d**, and the nanorods' diameter is from 230 to 500 nm (the average diameter is 360 nm); externally, disperse and ultrathin nanoflakes have grown along the ektexine of inside nanorods, the thickness of nanoflakes is about 60 nm, as shown in the inset of **Figure 2f.** Perpendicular grown smooth nanoflakes (*M*=0.2 M) have totally covered the inside nanorods, in **Figure 2g** and **Figure 2h**, whereas the thickness does not change clearly (~60 nm).

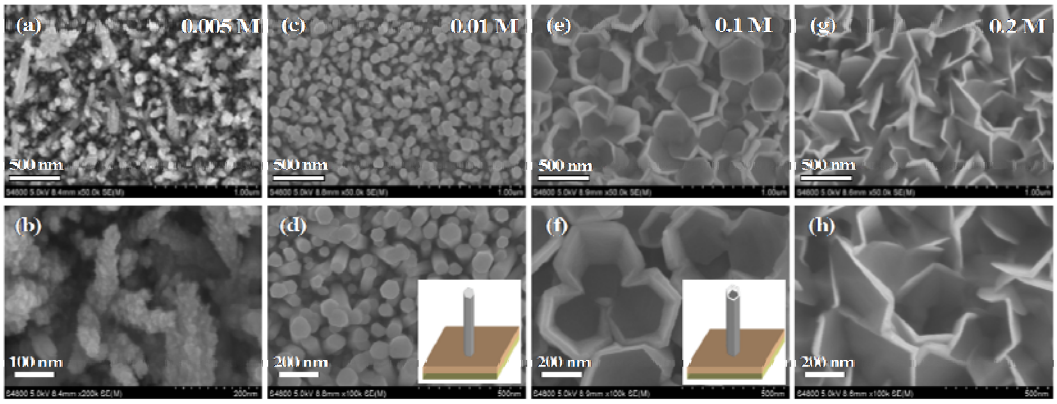

Figure 2. (Color online) SEM images of ZnO nanostructures

3.2. TEM

The morphologies for the samples were also obtained by the TEM images. **Figure 3a** shows the representative TEM image of the hierarchical ZnO nanostructure (*M*=0.2 M), which also confirms that the nanostructure has a hierarchical nanostructure: an outside nanoflake covers an inside nanorod; the thickness of nanoflakes is about 65 nm and the nanorods' diameter is about 600 nm. The homologous SAED pattern in the inset of **Figure 3a** shows discontinuous diffraction rings, which indicates that our samples are polycrystalline. It can be clearly seen from the HRTEM image of nanostructures in **Figure 3b** that ZnO nanostructures are well crystallized and the interplanar spacing as calculated from the HRTEM image is 0.26 nm, corresponding to the lattice constant of the standard hexagonal wurtzite structured ZnO in (001) plane.

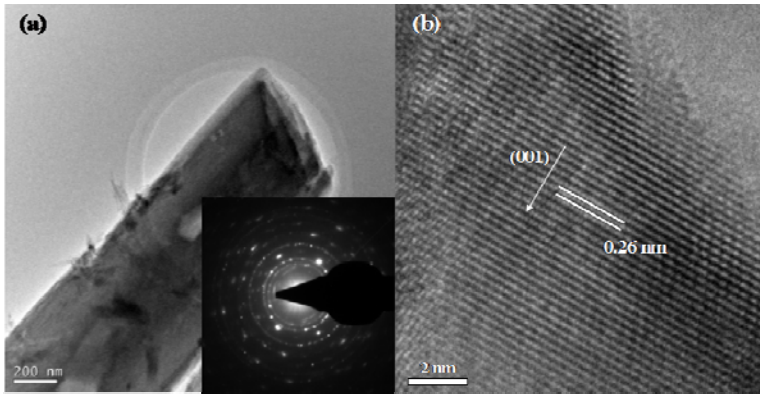

Figure 3. TEM and HRTEM images of ZnO nanostructures (*M*=0.2 M). (a) The representative TEM image and the inset is the SAED pattern. (b) The HRTEM image

3.3. XRD

The XRD patterns of grown ZnO nanostructures (*M*=0.005, 0.01, 0.015, 0.02 M) are shown in **Figure 4a**. The results indicate that all the peaks are indexed to the hexagonal wurtzite structure (JCPDS card No.36-1451) except the only wave packet come from the glass substrates. Any characteristic peak of other new phase is not detected, which indicates that all the ZnO nanostructures are single hexagonal wurtzite ZnO phase and have the high degree of crystallization. Prior to ZnO nanostructures growing, the ZnO buffer layer shows the excellent preferred (002) reflection (**Figure 4b**), suggesting the ZnO buffer layer has c-axis-preferred orientation perpendicular to the glass substrate surface [19]. What's more, as the increase of *M*, the intensity of the (002) peak of grown ZnO nanostructures from **Figure 4c** increases firstly, reaches the maximum value at *M*=0.1 M, and then decrease. Combining with SEM images, the shapes of grown ZnO nanostructures change from nanorods to nanorods covered by nanoflates with increasing of the concentration, when *M*<0.2 M nanorods grown along the c-axis direction becomes larger and larger as enhancing concentration, so the intensity of the (002) peak increases, whereas *M*=0.2 M that decreases instead, orient upwards nanoflakes totally covered the whole film should not grow along the c-axis direction.

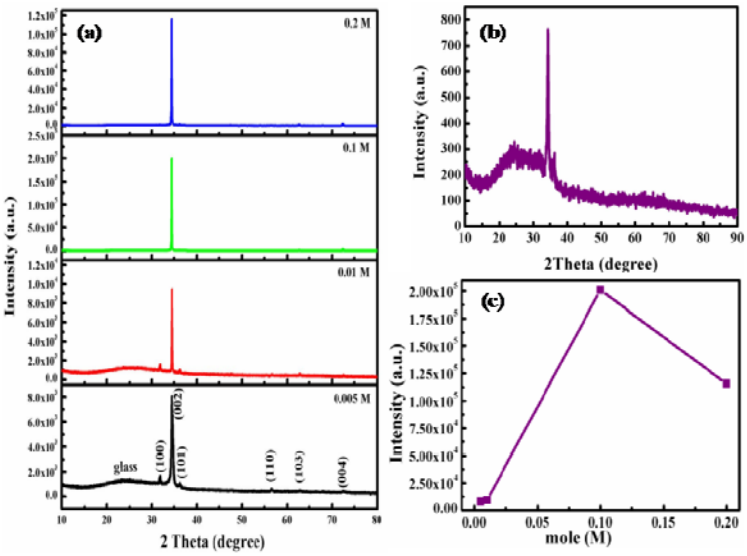

Figure 4. (Color online) (a) XRD patterns of grown ZnO nanostructures; (b) XRD pattern of the ZnO buffer layer; (c) Intensity of (002) peak of grown ZnO films

3.4. Raman

The additional optical information of ZnO nanostructures was obtained by Raman spectroscopy. **Figure 5** shows the RT Raman spectra of samples in the range of 100-800 cm^{-1}. The sole and obvious peak located at around 573 cm^{-1} can be assigned to A1 longitudinal optical (LO) mode [A_1(LO)], which is associated with the defects of oxygen vacancies, Zn-interstitials or their complex [8, 20, 21]. The intensity of A_1(LO) as function of concentration is shown in the inset of **Figure 5**, it's clear that the intensity of A_1(LO) monotonously enhances with the increase of the moles.

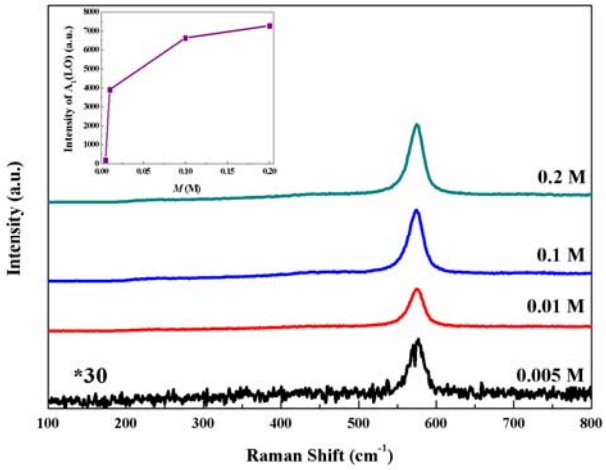

Figure 5. (Color online) Raman spectra of ZnO nanostructures. The inset is the intensity of A_1(LO) as function of concentration

3.5. UV-vis Absorption Spectra

The UV-vis absorption spectra of ZnO nanostructures synthesized at different moles are illustrated in **Figure 6a**. The optical band gap energy (E_g) can be estimated from absorption coefficient (α) using the Tauc relation:

$$\alpha h\upsilon = A(h\upsilon - E_g)^q$$

where A is a constant that depends on the transition probability, $h\upsilon$ is the energy of an incident photon, and q is an index that characterizes the optical absorption process. It is well known that direct and indirect band gap energy for the semiconductor nanostructures can be obtained from the intersection of linear fits of $(\alpha h\upsilon)^{1/q}$ versus $h\upsilon$ plots for q=1/2 and 2 on the x-axis [9]. ZnO is the direct bandgap semiconductor material, so we chose q=1/2 in the estimation. **Figure 6b**, based on **Figure 6a**, shows the plots of $(\alpha h\upsilon)^2$ vs $h\upsilon$ for ZnO nanostructures: the estimated values are about

3.32, 3.24, 3.23, and 3.25 eV, respectively, for different concentration (M=0.005, 0.01, 0.1, 0.2 M). The variation tendency of E_g is the same as that of the (002) peak intensity in the XRD spectra, so we suggest that E_g, as like the (002) peak intensity, strongly depends on grown ZnO nanostructures' shape: E_g decrease with enlarging nanorods, while increases when nanoflates appear in the surface.

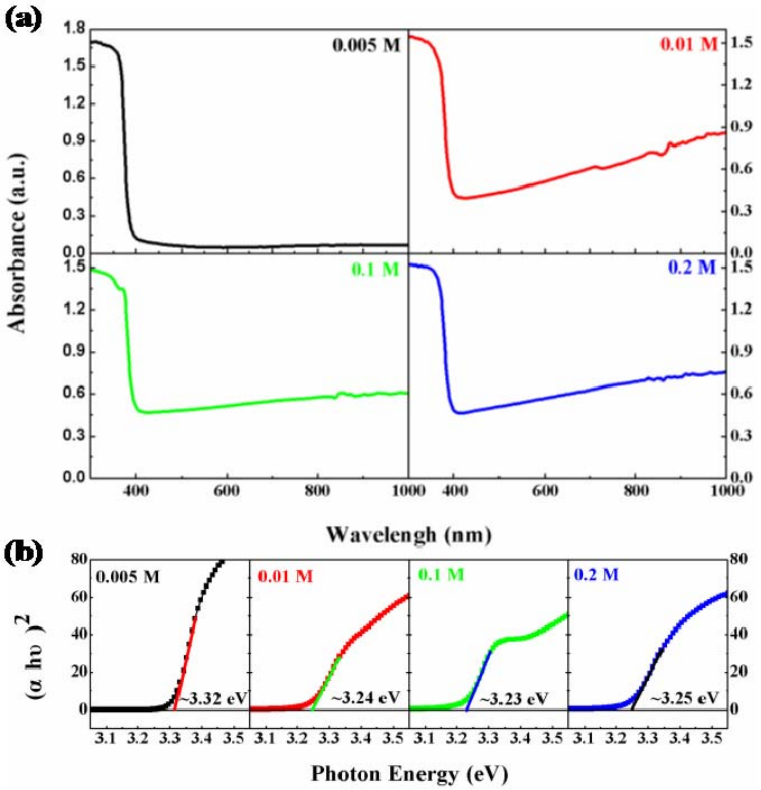

Figure 6. (Color online) (a) The UV-vis absorption spectra of ZnO nanostructures. (b) Plots of $(\alpha h\upsilon)^2$ vs $h\upsilon$ for ZnO nanostructures

4. CONCLUSIONS

ZnO nanostructures with different hierarchical nanostructures are prepared by the two-step hydrothermal method. SEM and TEM images show that as the increase of the concentration of the solutes the morphology of films change from hexagonal nanorods (irregular/regular) to hierarchical nanostrucure (nanorods covered by nanoflakes). XRD results show that all samples are the typical hexagonal wurtzite structure without any other new phase. In addition, Raman and UV-vis absorption spectra suggest that the optical properties strongly depend on nanostructures and morphology of ZnO.

5. ACKNOWLEDGEMENTS

This work is supported by National Science Fund for Distinguished Young Scholars (Grant No. 50925103 and 11034004), the Key grant Project of Chinese Minisitry of Education (Grant No. 309027), NSFC (Grant No.50902065) and the Fundamental Research Funds for the Central Universities (No. lzujbky-2012-28).

REFERENCES

[1] 3D Fe_3S_4 flower-like microspheres: high-yield synthesis via a biomolecule-assisted solution approach, their electrical, magnetic and electrochemical hydrogen storage properties
F. Cao, W. Hu, L. Zhou, W.D. Shi, S.Y. Song, Y.Q. Lei, S. Wang, and H.J. Zhang, Dalton Transactions 9246 (2009)

[2] Novel ZnO nanostructures over gold and silver nanoparticle assemblies
V. Pachauri, C. Subramaniam, and T. Pradeep, Chemical Physics Letters 423, 240 (2006)

[3] Effect of morphology on the solar photocatalytic behavior of ZnO nanostructures
M.S. Mohajerani, A. Lak, and A. Simchi, Journal of Alloys and Compounds 485, 616 (2009)

[4] On the growth mechanism and optical properties of ZnO multi-layer nanosheets
H.J. fan, R. Scholz, F.M. Kolb, M. Zacharias, U. Gosele, F. Heyroth, C. Eisenschmidt, T. Hempel, and J. Christen, Applied Physics A 79, 1895 (2004)

[5] Electrical properties of tin dioxide two-dimensional nanostructures
E. Comini, V. Guidi, C. Malagù, G. Martinelli, Z. Pan, G. Sberveglieri, and Z.L. Wang, Journal of Physical Chemistry B 108(6), 1882 (2004)

[6] Nanostructured stars of ZnO microcrystals with intense stimulated emission

Y.Z Lv, C.P. Li, L. Guo, Q.X. Wang, R.M. Wang, H.B. Xu, S.H. Yang, X.C. Al, and J.P. Zhang, Applied Phyisics Letters 87, 163103 (2005)

[7] Well-aligned arrays of vertically oriented ZnO nanowires electrodeposited on ITO-coated glass and their integration in dye sensitized solar cells
O. Lupana, V.M. Guérin, I.M. Tiginyanu, V.V. Ursaki, L. Chow, H. Heinrich, and T. Pauporté:, Journal of Photochemistry and Photobiology A: Chemistry 211, 65 (2001)

[8] Structural and spectroscopic characteristics of ZnO and ZnO:Er^{3+} nanostructures
A.K. Pradhan, K. Zhang, G.B. Loutts, U.N. Roy, Y. Cui, and A. Burger, Journal of Physics: Condensed Matter 16, 712 (2004)

[9] Synthesis, Magnetic Anisotropy and Optical Properties of Preferred Oriented Zinc Ferrite Nanowire Arrays
D.Q. Gao, Z.H. Shi, Y. Xu, J. Zhang, G.J. Yang, J.L. Zhang, X.H. Wang, and D.S. Xue, Nanoscale Res Lett 5, 1289 (2010)

[10] Ferromagnetism in ZnO Nanowires Derived from Electro-deposition on AAO Template and Subsequent Oxidation
J.B. Yi, H. Pan, J.Y. Lin, J. Ding, Y.P. Feng, S. Thongmee, T. Liu, H. Gong, and L. Wang, Advanced Materials 20, 1170 (2008)

[11] First-principles study of intrinsic point defects in ZnO: Role of band structure, volume relaxation, and finite-size effects
P. Erhart, K. Albe, and A. Klein, Physical Review B 73, 205203 (2006)

[12] Sol-gel synthesis and characterization of nanocrystalline ZnO powders
M. Ristic, S. Music, M. Ivanda, and S. Popovic, Journal of Alloys and Compounds 397, L1 (2005)

[13] Defect-Related Emissions and Magnetization Properties of ZnO Nanorods
B. Panigrahy, M. Aslam, D.S. Misra, M. Ghosh, and D. Bahadur, Advance Functional Materials 20, 1161 (2010)

[14] Room-temperature ferromagnetism in pure ZnO nanoflowers
X.F. Bie, C.Z. Wang, H. Ehrenberg, Y.J. Wei, G. Chen, X. Meng, G.T. Zou, and F. Du, Solid State Sciences 12, 1364 (2010) .

[15] Phase transformation and resistivity of dumbbell-like ZnO microcrystals under high pressure
C.L. Yu, Q.J. Yu, C.X. Gao, H.B. Yang, B. Liu, G. Peng, Y.H. Han, D.M. Zhang, X.Y. Cui, C.L. Liu, Y. Wang, B.J. Wu, C.Y. He, X.W. Huang, and G.T. Zou, Journal of Applied Physics 103, 114901 (2008)

[16] Hydrothermal growth of ZnO single crystals and their optical characterization
T. Sekiguchi, S. Miyashit, K. Obara, T. Shishido, and N. Sakagami, Journal of Crystal Growth 214/215, 72 (2000)

[17] Enzymatic glucose biosensor based on ZnO nanorod array grown by hydrothermal decomposition
A. Wei, X.W. Sun, J.X. Wang, Road, Y. Lei, X.P. Cai, C.M. Li, Z.L. Dong, and W. Huang, Applied Physics Letters 89, 123902 (2006)

[18] The effect of heating rate on the structural and electrical properties of sol-gel derived Al-doped ZnO films
M.Z. Gao, X.N. Wu, J. Liu, and W.B. Liu, Applied Surface Science 257, 6919 (2011)

[19] Structural and optical properties of Al-doped ZnO nanowires synthesized by hydrothermal method
S.N. Bai, H.H. Tsai, and T.Y. Tseng, Thin Solid Films 516, 155 (2007)

[20] Raman scattering and high temperature ferromagnetism of Mn-doped ZnO nanoparticles
J.B. Wang, G.J. Huang, X.L. Zhong, L.Z. Sun, Y.C. Zhou, and E.H. Liu, Applied Phyisics Letters 88, 252502 (2006)

[21] Radial ZnO nanowire nucleation on amorphous carbons
Y.H. Yang, C.X. Wang, B. Wang, Z.Y. Li, J. Chen, D.H. Chen, N.S. Xu, G.W. Yang, ┌ and J.B. Xu, Applied Phyisics Letters 87, 183109 (2005)